Multi-Modal Netted Sensor Fence for Homeland Security

Weiqun Shi, Ronald Fante, John Yoder, and Gregory Crawford,
The MITRE Corporation, 202 Burlington Road, Bedford, MA 01730

ABSTRACT

Potential terrorists/adversaries can exploit a wide range of airborne threats against civilian and military targets. Currently there is no effective, low-cost solution to robustly and reliably detect and identify low observable airborne vehicles such as small, low-flying aircraft or cruise missiles that might be carrying chemical, biological or even nuclear weapons in realistic environments. This paper describes the development of a forward-based fence that contains a multi-modal mix of various low cost, low power, netted sensors including unsophisticated radar, acoustic and optical (Infrared and visible) cameras to detect, track and discriminate such threats. Candidate target (Cessna, Beech Craft, crop duster, and cruise missile) signature phenomenologies are studied in detail through either theoretical, numerical simulation or field experiment. Assessments for all three modalities (Radar, acoustic and IR) indicate reasonable detectability and detection range. A multi-modal kinematic tracker is employed to predict the location, the speed and the heading of the target. Results from a notional, template based classification approach reveal reasonable discrimination between different aircraft tested in the field experiments.

Keywords: netted sensor fence, radar, Infrared, acoustics, detection, tracking and classification

1. INTRODUCTION

Potential terrorists/adversaries can exploit a wide range of airborne vehicles to effectively deliver weapons (nuclear, chemical and biological) against civilian and military targets. Candidate airborne threats may include low-radar-cross-section targets such as small civilian aircraft as well as cruise missiles that tend to fly low to elude conventional search radar detection. Given the large volume of airspace and the sheer number of potential targets in the United States and the difficulty of detecting and discriminating low observable airborne vehicles in realistic environments, there is currently no effective, reliable and low-cost solution for dealing with this threat.

This paper describes a low cost, low power (potentially disposable) methodology for performing key 24/7 sentry functions to protect critical civilian and military infrastructure from airborne threats. The methodology is based on joint multisensor exploitation technology by designing and developing a forward-based fence that contains a mix of various low cost, low power, netted sensors including an unsophisticated radar, acoustic microphones and optical (Infrared and visible) cameras to detect, track and discriminate potential airborne targets. An in-depth understanding of candidate target signature phenomenologies is developed through theoretical, numerical assessments and proof-of-concept field experiments. An integrated (over sensor modality) detection, tracking and discrimination process is developed which forms the basis of the fence's friend/foe sentry capability and ability to provide accurate/timely intercept information.

This paper is organized as follows. In section 2, we introduce the general system concept and design of the netted sensor fence showing how the sensors are arrayed relative to one another. In section 3 we focus on the detection issues which include assessments of detectablity and target signature phenomenology studies for all three sensor modalities through either theoretical analysis, numerical simulation or direct measurement via field experiment. A kinematic tracker development using standard Kalman filtering is discussed in section 4. Classification algorithms and results are presented in section 5, followed by a brief conclusion.

2. SYSTEM CONCEPT AND DESIGN

The forward-based sensor fence system and associated sensors is designed to be low cost, low power, and highly portable. A conceptual illustration of the system is shown in Figure (2-1).

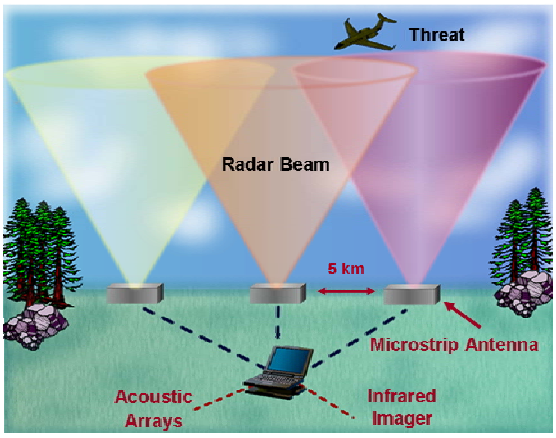

Figure 2-1. A conceptual illustration of the netted sensor fence for airborne threat detection, tracking and classification.

The primary detection component in the system is a radar fence. The radar fence is designed to detect approaching targets and provide a cue to the acoustic and infrared sensors that perform the discrimination task. The radar fence consists of multiple, low power (10 Watts), non-scanning (for low cost and complexity), UHF, pulse-Doppler radars (to estimate target speed, range and eliminate birds and ground clutter), with a radar-to-radar separation of approximately 5 km (Figure 2-1). Each radar operates with a different carrier frequency (to avoid crosstalk between radars) and has a beamwidth that is broad in both azimuth (so that the number of radars can be kept small) and elevation (to detect both high and low-flying targets). The radars measure target range and radial speed five times per second and report these values to a central processing station that cues the acoustic and infrared sensors (if a target report is issued), and then fuses the reports from all sensors (radars, acoustic, etc.) to form a target track and alert rear-area weapons systems or potential interceptors so that defensive action can be taken. A complete description of the radar parameters and detection characteristics is contained in Tables 2-1 and 2-2.

Type	Pulse/Doppler
Frequency	UHF
Scan	None (Radar Stares Forward)
Antenna	Broadbeam, Gain $\simeq$ 3 dB
Polarization	Circular
Average Power	10 W
Duty Factor	10%
Pulse Repetition Frequency	10 kHz
Coherent Integration Time	0.2 sec. (5 Hz Update Rate)
Unambiguous Range	75 km
Unambiguous Speed	750 m/sec
Range Resolution	150 m
Speed Resolution	1.9 m/sec
Minimum Detection Range	25 km
Range for Probability Detection = 0.9	7 km (Small Target), 15 km (Large Aircraft)
Noise-Induced False Alarm Rate	1 Per Month
Clutter/Bird Cancellation Approach	Blank Lowest few Doppler Bins
Quantities Measured	Target Range and Speed (Azimuth and Height Estimated)
Target Discrimination	Based on Speed Only. Need Other Sensor Types

Table 2-1. Individual Radar Properties

Acoustic microphone arrays are used as the second sensor modality in the system to detect broadband acoustic emissions from approaching targets. Acoustic sensors are non-line-of-sight, passive, low-cost, and portable sensors that can be effectively deployed in wide areas. Primary objectives of acoustic sensors in this sensor fence system are: 1) to provide target direction of arrival (DOA) estimates that will then be fused with radar measurements to form a target track; 2) to provide a means for target identification and classification; and 3) to mitigate false alarms. The system is designed to contain several equally spaced, 8-element diagonally-arranged microphone arrays between the radar sensors.

The third sensor modality in the fence is an optical system which is cued by the radar and/or acoustic sensors and slews in angle to acquire, track and identify the potential airborne threat. The system is designed to contain an uncooled infrared detector sensitive to the 8-12 μm waveband to provide day and night time operation. The uncooled IR detector array uses only several Watts of power. A boresighted visible camera is also used for improved target resolution during the daytime. Visible cameras are inexpensive and have improved resolution compared to the infrared detector array.

Radar Separation	5 km
Radar-Frequency Separation (to Avoid Crosstalk)	1 MHz
Communications Links	Only to Central Processor (No Radar-to-Radar Links)
Target Information Fusion (from Radars, Acoustic, etc.)	Kalman Filter Estimates Target Track

Table 2-2. Radar Fence Properties

3. DETECTION

3.1 Radar Detection

Assessments of radar detectability and detection range are accomplished via numerical simulation. In Table 2-1, the range at which the probability of detection equals 0.9 was calculated assuming a non-fluctuating target (this is why the UHF frequency band was chosen), with the signal-to-noise ratio at target range R calculated from,

$$\frac{E}{N_o} = \frac{PG^2\sigma\lambda^2\tau}{(4\pi)^3 R^4 k T_o F L}, \qquad (3\text{-}1)$$

for ranges where the target is completely uneclipsed (eclipsing occurs if part or all of the return from the target is received while the transmit pulse is still on), which implies $R > cT/2$, where c = speed of light and T = duration of the uncompressed radar pulse. Also, P = average transmitted power, G = antenna gain at the target (this varies with target location), σ = target radar cross section, τ = coherent integration time, λ = wavelength, k = Boltzmann's constant, T_0 = 290°K, L = loss, and F = receiver noise figure. When the target is partially eclipsed, the signal-to-noise ratio in Equation (3-1) is reduced by (2R/cT). The pulse repetition frequency was chosen so that the radar is unambiguous (unambiguous range = $c/2\cdot PRF$, unambiguous speed = $\lambda\cdot PRF/2$) in both target range and speed for all targets of interest. Plots of E/N_0 (including antenna patterns) for a target with a 3 m^2 radar cross section flying at 100 m altitude and crossing the fence directly above radar (X = 0) and at 2 km from radar are shown in Figure 3-1. These values were used with the standard curves [1] of probability of detection per look versus signal-to-noise ratio to calculate the probability, Pd(n), that the target is detected at the end of the coherent integration interval τ at a time when the target is at a range R_n. Finally, the cumulative probability that the target has been detected by the time it reaches range R_m is

$$P_c(m) = 1 - \prod_{n=0}^{m} \left[1 - P_d(m)\right], \qquad (3\text{-}2)$$

where R_0 (n = 0) corresponds to the range at which the target comes over the horizon. The range R_m where Pc(m) = 0.9, for the case when X = 2 km, is the value cited in Table 2-1.

3.2 Acoustic Detection

Acoustic detection assessments are primarily accomplished by performing several field measurements of different types of aircraft to obtain information on target acoustic detection and signature characteristics. Although many aircraft

acoustic data are available in literature [2,3], however, for the purpose of developing and testing multi-modal sensor fence detection, tracking and classification algorithms, it is critical to simultaneously obtain data measurements from all the fence sensors at the same time. A typical experiment layout and the 8-element acoustic microphone array (with equal element spacing of 0.5m) are shown in Figure (3-2). The sensor suite which includes acoustic array and IR/visible cameras are positioned near the end of an airport runway. The test aircraft are flying at a flight test matrix with multiple combinations of altitude and engine RPM. GPS data recording systems are mounted on the aircraft so the ground truth information can be retrieved and later can be used for target validation after the flight. Since the primary targets of interest in this study are small, low-flying civilian aircraft, realistic candidate aircraft have been tested , as shown in Figure (3-3), which include a three-blade crop duster, a two-blade crop duster, a twin engine Beech Craft, and a single engine Cessna 172.

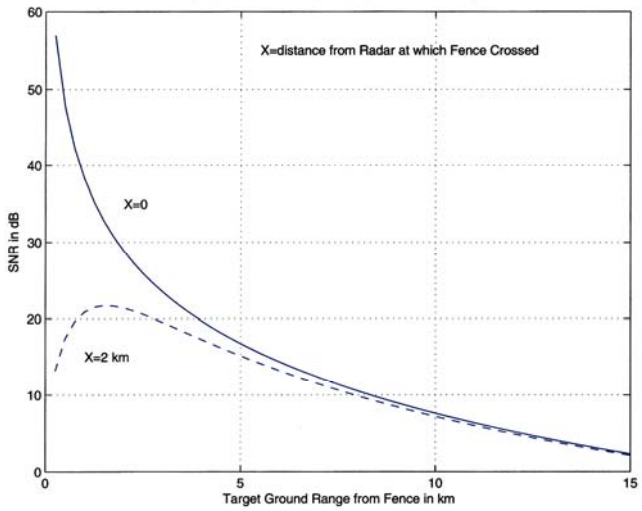

Figure 3-1. SNR for Low-Flying Target with a Radar Cross Section = 3 m^2

Figure (3-4) shows a spectrogram of a measured acoustic data showing a rich array of features corresponding to two crop dusters flying above the sensor array. Strong Doppler shifted harmonic structures caused by aircraft' engine noise are observed. The parabolic energy distortion (in the time period between 60-80 seconds) in the spectrum is caused by the multipath ground reflection interference when the target is passing directly above the sensor array. The spreading width of the parabolas is directly related to the speed of the targets.

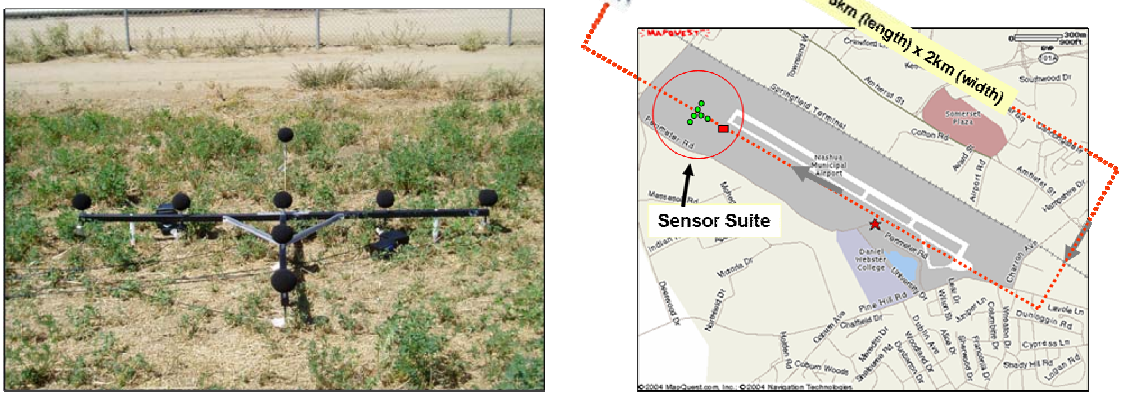

Figure 3-2. Field experiment set up (right) and the acoustic microphone array (left)

Figure 3-3. Two crop dusters, a twin engine Beech Craft and a single engine Cessna 172 have been tested in the experiments.

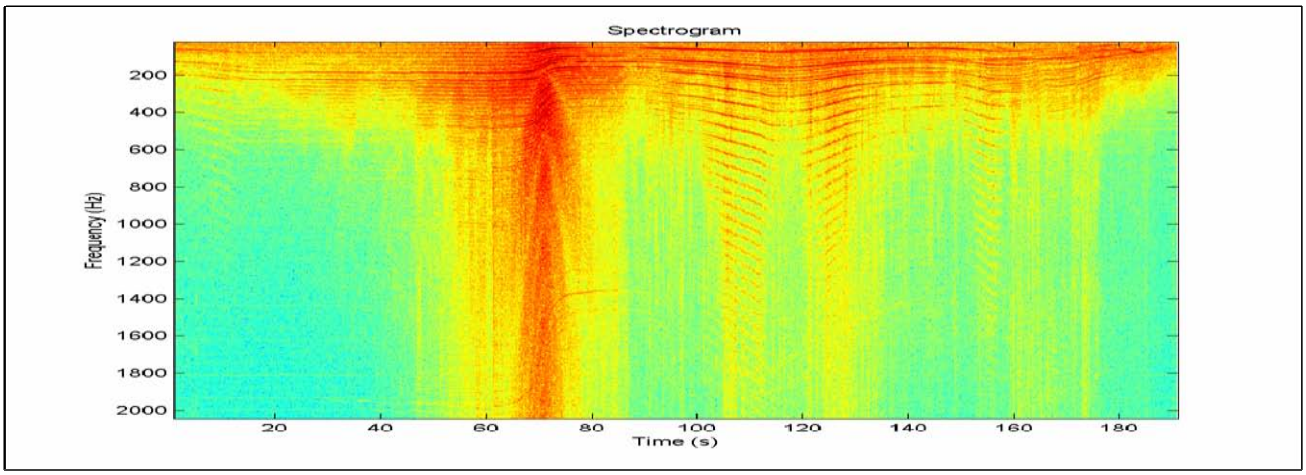

Figure 3-4. Spectrogram of two crop dusters flying above the sensor array

3.3 IR Detection

The activities we undertook to design and optimize this system started with an evaluation of IR detectors, wavebands and target signatures. During this process we calculated the effective range of these IR systems. This work was followed by designing an experimental set-up and experiments to collect images of airborne targets.

Detector received power for an optical system whose diameter is D, pixel angular field-of-view is $\delta\phi$, target range is R and target spectral radiance is $J(\lambda)$ W/Sr/μm is calculated below. The backgrounds are clouds and atmospheric aerosol scattering. The magnitude of these backgrounds can be calculated by MODTRAN [4] runs for any specific defined atmospheric condition.

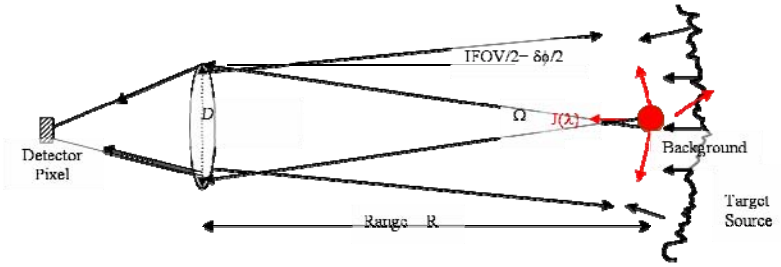

Figure 3-5. Diagram of the Optical System and the Target Environment

The signal power received from the source by the detector is given by

$$P_S = \int_{\lambda_1}^{\lambda_2} T_{optics} T_{atmosphere}(\lambda) J(\lambda) * \frac{\pi D^2}{4R^2} d\lambda = \frac{\pi D^2}{4R^2} T_{optics} \int_{\lambda_1}^{\lambda_2} T_{atmosphere}(\lambda) J(\lambda) * d\lambda \qquad (3\text{-}3)$$

Where T_{optics} is the transmittance (or transmission coefficient) of the optical system and $T_{atmosphere}$ is the transmission of the atmosphere along the path from the source to the sensor. Generally, with proper optics design, the transmission of the optics is a constant independent of wavelength, but the transmission of the atmosphere is a function of wavelength. The integration is performed over the spectral bandpass of the optical system. This derivation assumes that the source is incident on a single pixel. The expression can be approximately corrected for multiple pixels on the target by dividing by the number of pixels on the target, n.

The power on each detector pixel from the background scene in the field-of-view of each pixel (see figure) is given by

$$P_B = (IFOV)^2 \frac{\pi D^2}{4} T_{optics} \int_{\lambda_1}^{\lambda_2} T_{atmosphere}(\lambda) N_{background}(\lambda) d\lambda \qquad (3\text{-}4)$$

where, IFOV is the instantaneous angular field of view of each square pixel (radians) and $T_{atmosphere}*N_{background}$ is the background spectral radiance W/(Sr cm^2 μm) at the aperture. The term $T_{atmosphere}*N_{background}$ can be obtained from the MODTRAN atmospheric modeling code and already contains the effects of atmospheric transmission between the noise sources (background scene and/or aerosol scattering) and the receiver aperture. Thus optic transmission term can be dropped from the expression. Note: R and D have units of centimeters, and λ has units of μm.

The circuit power is proportional to the square of the current so, the power signal to noise ratio is given by [5],

$$\left(\frac{S}{N}\right)_P = \frac{i_S^2}{\left(i_N^2\right)_{Mean}} = \frac{\eta^2 e^2 P_S^2}{(h\nu)^2} * \frac{h\nu}{2\eta e^2 \left(P_S + P_{B'}\right)} = \frac{\eta P_S^2}{2h\nu B\left(P_S + P_{B'}\right)} \qquad (3\text{-}5)$$

For the typical infrared case of the signal power being much less than the background power $P_s << P_{B'}$, (background limited detection) then

$$\left(\frac{S}{N}\right)_P = \frac{\eta P_S^2}{2h\nu B P_{B'}} \qquad (3\text{-}6)$$

[Note: the background power, $P_{B'}$, is due to all non-signal sources, including (a) nearby detector cryogenic Dewar radiation, (b) optics radiation, (c) radiation from the field-of-view limiting shrouds and (d) other nearby sources]. We can invoke the "pure detection" criterion [6] that if the signal to noise ratio with the target in a pixel minus the signal to noise ratio with the target not in the pixel ($SNR=SNR_{target}-SNR_{no\text{-}target}$) is greater than 5, the target will be detected against a cluttered background. The range of detection of an airborne target at various altitudes can then be calculated and the results are shown in Figure 3-6.

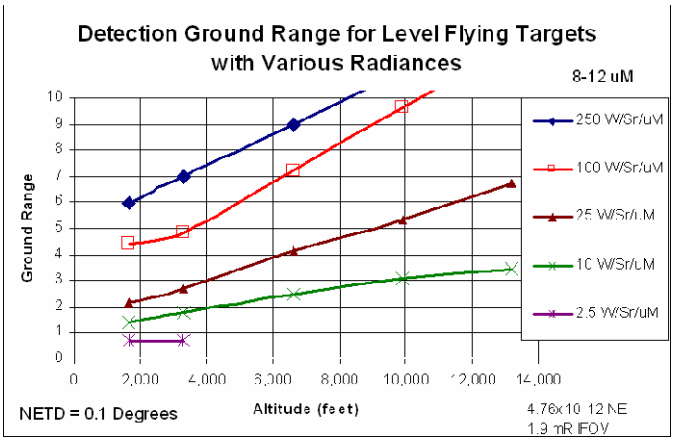

Figure 3-6. Attitude and ground range for the detection of airborne targets of various values of target radiance.

This calculation is for an uncooled 8-12 μm detector with a noise equivalent temperature difference (NETD) of 0.1 degrees and shows the altitude and ground range for the detection of airborne targets of various values of target radiance. Typical aircraft have spectral radiance of about 100 W/Sr/μm so targets can be detected at ranges in excess of 5 km even if they are at low altitudes. (Note a NEI of 0.1 degrees corresponds to a NEI of about 4.76×10^{-12} W/cm^2 for a 1.9 milliradian IFOV.)

The experimental set-up to collect visible and IR field data is shown in Figure 3-7. The visible and IR cameras are boresighted with each other to take simultaneous visible and IR images of the target. A frame grabber and computer is used to collect the data and display the images side-by-side.

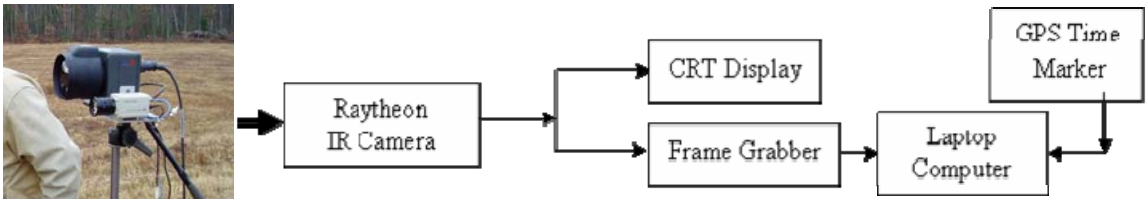

Figure 3-7. IR/visible data collection set up.

The IR camera is a BAE 320x280 micro-bolometer array which is sensitive over the wavelength range of 7 to 14 μm. The FOV of the array is 7.7x10.3 degrees and the IFOV of each pixel is about 0.56 milliradians. It has a NETD of aboutabut 0.08 Celsius and consumes only 6 Watts of power.

Typical images at short range are shown in Figure 3-8 at the lower left for a Cessna and the middle for a crop duster. The detection of a twin engine Cessna is at 6.1 km shown at the lower right.

Figure 3-8. The detection of single engine Cessna (left), a crop duster (middle) and a twin engine Cessna at 6.1 km (right)

4. TRACKING

The system employs a Kalman filter to establish multi-target tracks using radar and acoustic measurements as input. The tracker is designed to handle multiple targets and false reports. It is also designed to have data input flexibilities such as allowing input data measurements from each sensor (radar and acoustic) that are not time coordinated. The tracker must allow that some tracks it creates may be based on false reports, and therefore these tracks must be dropped if they behave erratically or do not associate with further detections at later times. Tracks can be promoted or demoted by evaluating cumulative properties of a score that was originally assigned to the initial tracks. Constant velocity with additive white noise acceleration is introduced in the plant noise assumption. Since the range of radar measurements is on the order of ~10 km, it is adequate to use a flat earth model when calculating tracker updates.

An example of track generation and its performance is depicted below in Figure (4-1). In this example a set of simulated radar range measurements r1, r2, r3 from three adjacent radars are combined with an actual acoustic measurement of target azimuth and elevation angles as input to form a track. The data segment consists of nine seconds of data with a data spacing of 0.125 seconds (8 Hz). Input and output results from the tracker in Figure (4-2) are broken down as follows: (a)-(b)-the measured (dotted line) and the estimated (solid line) azimuth and elevation angles; (c)-(e) – the

simulated (dotted line) and the estimated (solid line) radar range parameters r1, r2 and r3; (f)-the estimated position coordinates and the estimated and ground truth range comparisons; (g)-output of target velocities.

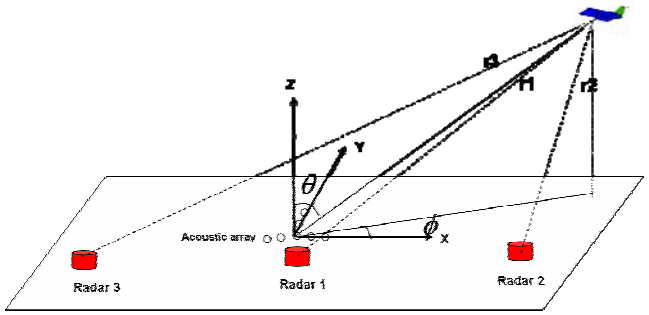

Figure 4-1. Geometry for the sensor fence tracking problem

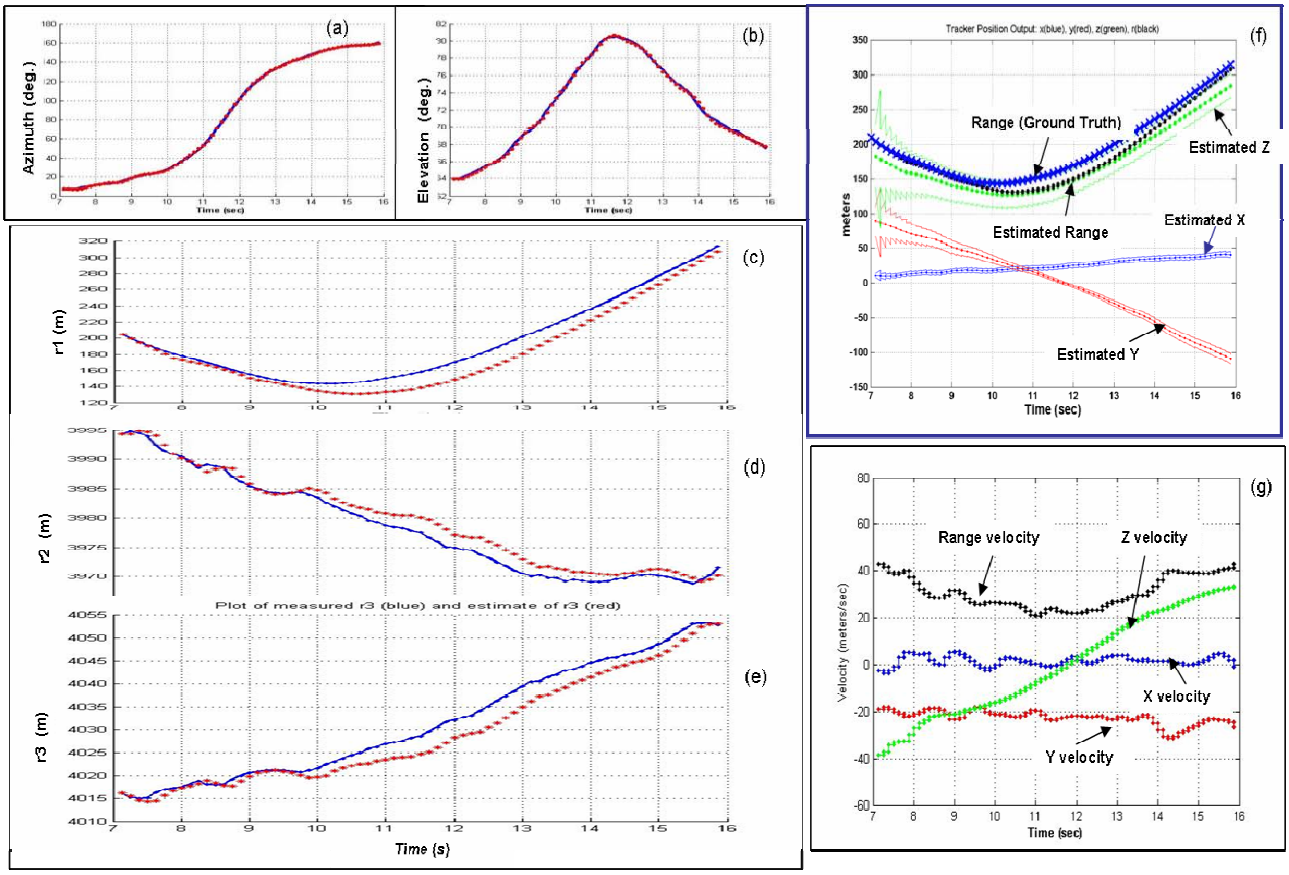

Figure 4-2. Input and output comparisons of the kinematic tracker.

5. CLASSIFICATION

In this sensor fence system target classification tasks are shared by all three sensor modalities. Through the sensor fusion process using radar and acoustic data a track which indicates the kinematic properties of approaching targets is formed. Information such as target velocity, range and location can be extracted from the tracker to give an initial classification of target types. Acoustic measurements can be used to further divide the target groups. Therefore targets such as typical false alarms (e.g., birds, ducks, etc.), propeller driven aircraft (civilian small aircraft), helicopters, and

jets can be classified. A further classification which has the potential to discriminate similar target types, e.g. a single engine Cessna vs. a twin engine Beech Craft can be achieved via the use of IR/visible image classification. The following sections give detailed descriptions of the classification approach used in this netted sensor system.

5.1 Acoustic Feature Extraction and Classification

As mentioned earlier, the primary targets of interest in this study are small, low-flying aircraft. Such small aircraft tend to emit strong harmonic lines produced by propeller or propfan noise. This suggests that a target classification algorithm can be developed based on the Harmonic Line Association (HLA) method.

Given an acoustic time sequence and the corresponding sampling rate, an FFT spectrum is computed at each buffered data frame. A noise spectrum is calculated using a two-pass notched moving average approach with a single-sided window width and a given detection threshold estimated from past experimental data. Spectra peaks, defined as a sequence of 3 FFT bins where a local max occurs are then detected, and the frequencies at which the peaks are detected are accurately determined by doing a parabolic curve fitting to the peak profiles. Using the most significant peak as an anchor, those harmonically related frequency peaks are grouped together to form a hypothetical harmonic feature vector set. This process is then repeated until all the harmonic feature vector sets are extracted for each data frame from all the frames available. It has been found from the field experiments that the most informative aircraft harmonic signatures for small civilian aircraft usually exist within the frequency range from 20-2000 Hz. Given a typical fundamental frequency of small civilian aircraft that are on the order of 50 Hz during normal flight, the first 40 harmonics are selected to form a 40-component feature vector which will be used for the classification. In order to minimize the sound propagation effect and make the feature vector essentially distance invariant, the magnitude of each component is normalized relative to the sum of the magnitudes of the two highest harmonics in the set. Finally the derived feature vectors from each data frame are statistically averaged to form a feature vector template which distinctively represents the aircraft target . The above workflow is summarized in Figure 5-1.

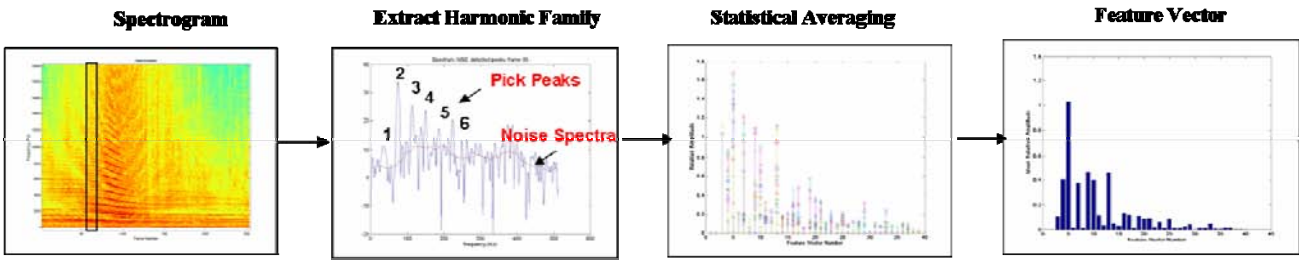

Figure 5-1. Acoustic feature extraction process

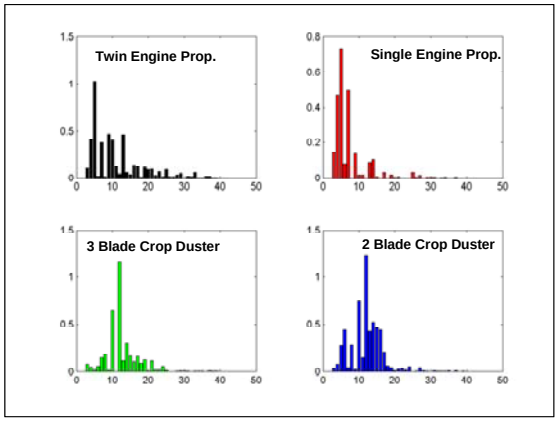

Figure 5-2. Normalized feature vector template for the four different aircraft tested in the experiments.

Feature vectors generated for four aircraft tested in the experiment are shown in Figure 5-2. The final classification is performed using a Nearest Neighbor classifier.

5.2 IR Feature Extraction and Recognition

Aircraft recognition from IR images is done based on the Moment Invariants method. The Moment Invariants method has been frequently used as a feature extraction technique for image processing, remote sensing, shape recognition and classification [7]. The method extracts a set of numerical attributes - the moment feature vectors which uniquely characterize the shape of an object and yet have the desired property of invariance under image translation and rotation. The method was first applied to aircraft shape identification from binary television images by Dudani, etc. [8] and was shown to be quick and reliable.

The mathematical foundation of Moment Invariants for two-dimensional shape recognition was first introduced by Hu [9], in which a set of shape descriptor values were computed from central moments through order three that are independent to object translation, scale and orientation. Translation invariance is achieved by computing moments that are normalized with respect to the centre of gravity so that the centre of mass of the distribution is at the origin (central moments). Size invariant moments are derived from introducing a simple size normalization factor. From the second and third order values of the normalized central moments a set of invariant moments can be computed which are independent of rotation.

In this paper six invariant moment functions that appear to be suitable for the present problem are selected with their mathematical expressions given below,

$$
\begin{aligned}
M_1 &= ((\mu_{20}-\mu_{02})^2 + 4\mu_{11}^{\ 2})/r^4 \\
M_2 &= ((\mu_{30}-3\mu_{12})^2 + (3\mu_{21}-\mu_{03})^2)/r^6 \\
M_3 &= ((\mu_{30}+\mu_{12})^2 + (\mu_{21}+\mu_{03})^2)/r^6 \\
M_4 &= ((\mu_{30}-\mu u_{12})(\mu_{30}+\mu_{12})\cdot[(\mu_{30}+\mu_{12})^2 - 3(\mu_{21}+\mu_{03})^2] \\
&\quad + (3\mu_{21}-\mu_{03})(\mu_{21}+\mu_{03})\cdot[3(\mu_{30}+\mu_{12})^2 - (\mu_{21}+\mu_{03})^2])/r^{12} \\
M_5 &= ((\mu_{20}-\mu_{02})\cdot[(\mu_{30}+\mu_{12})^2 - (\mu_{21}+\mu_{03})^2] + 4\mu_{11}(\mu_{30}+\mu_{12})(\mu_{21}+\mu_{03}))/r^8 \\
M_6 &= ((3\mu_{21}-u_{03})(\mu_{30}+\mu_{12})\cdot[(\mu_{30}+\mu_{12})^2 - 3(\mu_{21}+\mu_{03})^2] \\
&\quad + (\mu_{301}-3\mu_{12})(\mu_{21}+\mu_{03})\cdot[3(\mu_{30}+\mu_{12})^2 - (\mu_{21}+\mu_{03})^2])/r^{12}
\end{aligned}
\tag{5-1}
$$

Where $\mu_{pq} = \frac{1}{N}\sum_{i=1}^{N}(u_i-\bar{u})^p(v_i-\bar{v})^q$ are the central moments, u and v are the image coordinates, and $r=\sqrt{(\mu_{20}+\mu_{02})}$ the gyration factor which is used to normalize the moment functions in order to obtain the desired size invariance.

A preprocessing of IR images is performed before the final recognition process. After detection, the area that contains the potential target is first cropped from the original image. Then a binary image is formed by a simple threshold circuit. The aircraft silhouette is next extracted from the resulting binary image and its coordinates are used for the invariance moments feature vector exaction. Figure (5-3) illustrates the above workflow.

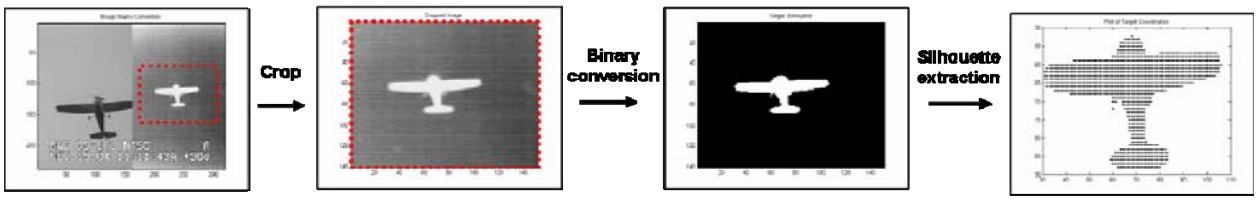

Figure 5-3, IR image preprocessing workflow for target classification

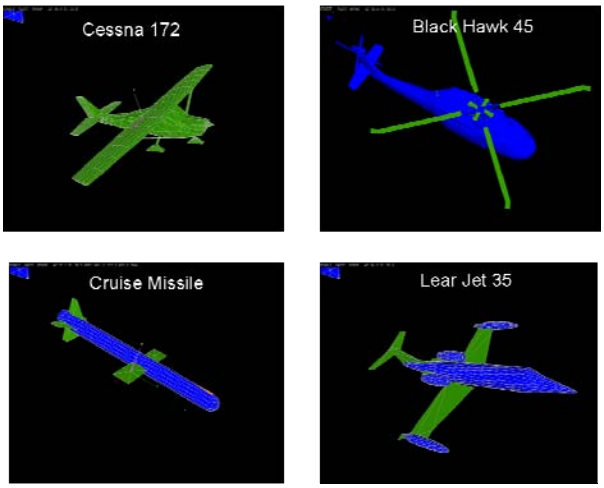

Figure 5-4. Three-dimensional models used in IR image classification

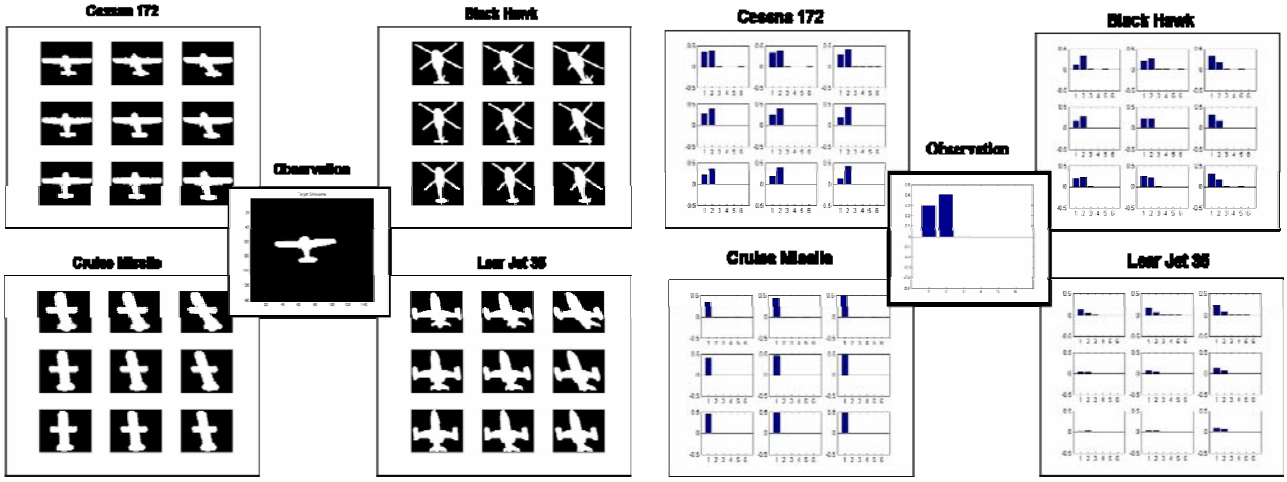

Figure 5-5, A measured IR image (center) and the projected 2D images of the selected aircraft (left plot), and the extracted invariant moment vectors (right plot)

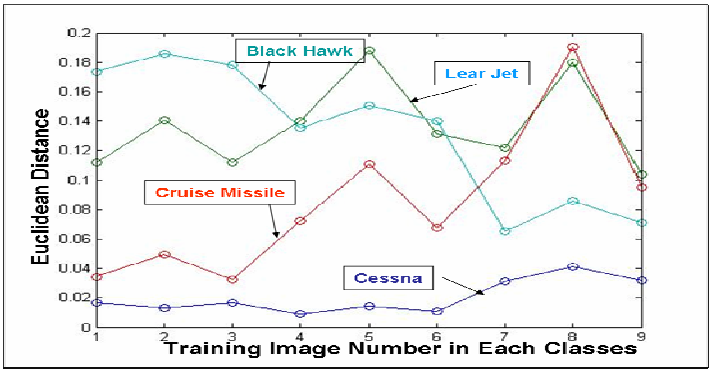

Figure 5-6 Euclidean distances suggests a good confidence level of the classification result, in which a Cessna 172 aircraft is clearly identified.

To perform an initial classification test, a collection of numerically generated three-dimensional models representing classes of targets of interest (small civilian aircraft, military helicopters, large jets, and cruise missiles) were chosen to be compared against the IR image collections from the field test. The three-dimensional models, as shown in Figure (5-4), consist of a Cessna 172, a Black Hawk helicopter, a Lear jet 35, and a cruise missile Short. These models are constructed based on scaled drawings of the geometric models of each type.

In order to compare the candidate target templates to the observed IR images, the corresponding three-dimensional models must be projected into a two-dimensional image plane with the appropriate azimuth ϕ and elevation θ angles corresponding to the camera viewing angles. Taking advantage of the multi-modal sensor character, the azimuth and the elevation angles can be effectively determined from the output of the kinematic tracker derived from the corresponding radar and acoustic measurements. Since the tracker provides the kinematic parameters of the target which include the range, the angles of arrival, and the flight trajectory, the perspective azimuth and elevation angles (ϕ, θ) of the target can be derived from a simple geometrical translation. Figure (5-5) shows an example of a measured IR image and the projected 2D images centered on the observed azimuth and elevation (ϕ=110, θ=60) with variations of ±10 degrees on both angles. The corresponded invariant moments are extracted from these images and the results are also shown in the figure.

A nearest neighbor classifier is then applied to train the extracted features and the final classification results can therefore be obtained. Euclidean distances between the moment vectors extracted from the observed IR images and those from the suspected 3D numerical models can be used to measure the confidence level of the classification results, as shown in Figure 5-6. In the case, the Cessna 172 target is correctly identified from the candidate set of potential target templates.

6. CONCLUSION

Small, low-flying airborne threat detection is an important component in anti-terrorism and homeland defense. Using a forward-based fence that contains a mix of low cost, low power radar, acoustic and optical (Infrared and visible) sensors it is feasible to detect, track and discriminate small, low flying airborne targets and provide 24/7 sentry functions to protect critical civilian and military infrastructure.

7. ACKNOWLEDGEMENTS

The authors thank Gus Arabadjis, Jeff Atwood, Chris Bas, Bryan George, Peter Hill, Garry Jacyna, Mike Jeffris, Walter Kuklinski, Tim Nadeau, Michael Otero, Richard Plasse, Dennis Reeves, Lucien Teig, and Stephen Theophanis for their contributions to this project.

REFERENCES

1. Skolnik, M., Radar Handbook (Second Edition) ,Chapter 2,McGraw-Hill(New York) 1990
2. Ferguson BG, Lo KW., “Turboprop and rotary-wing aircraft flight parameter estimation using both narrow-band and broadband passive acoustic signal-processing methods”, J Acoust Soc Am. 2000 Oct;108(4):1763-71
3. T. Pham, N. Srour, “TTCP AG-6: Acoustic Detection and Tracking of UAVs”, Proc. Of SPIE Vol. 5417, 24-30
4. MODTRAN code, Air Force Research Laboratory, http://www.vs.afrl.af.mil/Division/VSBYB/modtran4.html
5. R.H. Kingston “Detection of Optical and Infrared Radiation” by, Springer-Verlag, Pages 15-17, 1978
6. James D. Howe, “Electro-Optical Imaging System Performance Prediction”, Volume 4, Infrared and Electro-Optical Systems Handbook, Page 85 SPIE Engineering Press, Second Printing (1996)
7. Laura Keyes, Adam Winstanley, “APPLYING COMPUTER VISION TECHNIQUES TO TOPOGRAPHIC OBJECTS”, IAPRS, Vol. XXXIII, Amsterdam, 2000
8. S. A. Dudani, K. J. Breeding, and R. B Mcghee, “Aircraft Identification by Moments Invariants”, IEEE Transactions on Computers, Vol. C-26, No. 1 1977
9. M. K. Hu, “Visual Pattern Recognition by Moment Invariants”, IRE Trans. Inform. Theory, Vol. IT-8, 179-187, Feb. 1962